Suspended phospholipid bilayers: A new biological membrane mimetic

Graphical Abstract

Suspended phospholipid bilayers: a new biological membrane mimetic

Sophie E. Ayscough, Luke A. Clifton, Maximilian W. A. Skoda, Simon Titmuss

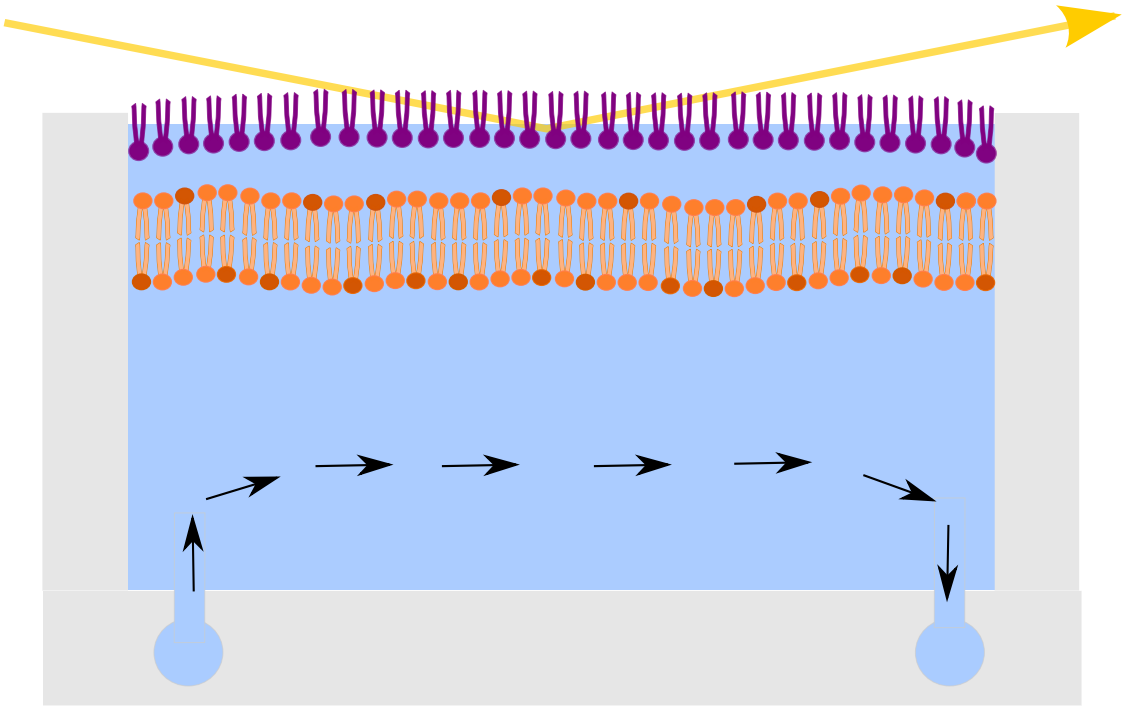

Suspended phospholipid bilayers: a new biological membrane mimetic

Sophie E. Ayscough[a,1], Luke A. Clifton[b], Maximilian W. A. Skoda[b], Simon Titmuss[a,*]

[a]*School of Physics & Astronomy, University of Edinburgh, James Clerk Maxwell Building, Peter Guthrie Tait Road, Edinburgh, EH9 3FD, UK*
[b]*ISIS Neutron & Muon Source, Rutherford Appleton Laboratory, Harwell Oxford, OX11 0XX, UK*

Abstract

Hypothesis

The attractive interaction between a cationic surfactant monolayer at the air-water interface and vesicles, incorporating anionic lipids, is sufficient to drive the adsorption and deformation of the vesicles. Osmotic rupture of the vesicles produces a continuous lipid bilayer beneath the monolayer.

Experimental

Specular neutron reflectivity has been measured from the surface of a purpose-built laminar flow trough, which allows for rapid adsorption of vesicles, the changes in salt concentration required for osmotic rupture of the adsorbed vesicles into a bilayer, and for neutron contrast variation of the sub-phase without disturbing the monolayer.

Findings

The neutron reflectivity profiles measured after vesicle addition are consistent with the adsorption and flattening of the vesicles beneath the monolayer. An increase in the buffer salt concentration results in further flattening and fusion of the adsorbed vesicles, which are ruptured by a subsequent decrease

*Corresponding author
Email address: simon.timuss@ed.ac.uk (Simon Titmuss)
[1]Now at European Spallation Source, Lund, Sweden

in the salt concentration. This process results in a continuous, high coverage, bilayer suspended 11 Å beneath the monolayer. As the bilayer is not constrained by a solid substrate, this new mimetic is well-suited to studying the structure of lipid bilayers that include transmembrane proteins.
Abbreviations: Neutron Reflectivity, NR; Area Per Molecule, APM; Supported Lipid Bilayers, SLBs; attenuated total reflectivity infrared spectroscopy, ATR-IR; Quartz Crystal Microbalance with Dissipation, QCM-D; Langmuir-Blodgett, LB; Floating Supported Bilayers, FSBs; Self Assembled Monolayer, SAM; Dimethyldioctadecylammonium bromide, DODAB; 1-palmitoyl-2-oleoyl-sn-glycero-3-phosphocholine, POPC; 1-palmitoyl-2-oleoyl-sn-glycero-3-phospho-(1'-rac-glycerol)(sodium salt), POPG); Mechanosensitive Ion Channel of Large Conductance, MscL.

Keywords: lipid bilayer, interface, membrane, vesicle rupture, neutron reflectivity keyword one, keyword two

---

1. Introduction

Planar lipid bilayers are a useful platform to investigate the physical characteristics of biological membranes. They can be used to investigate interactions between membranes and drug molecules and the response of membranes to physical stimuli [1, 2, 3, 4, 5]. Research into bacterial membranes as drug targets for antimicrobial treatments has led to the development of several planar mimetic systems which facilitate investigation by surface sensitive techniques [6, 7, 8].

Membrane models comprised solely of lipids or lipid mixtures are an important tool for understanding membrane biophysics [9, 10]. Such systems are drastically simplified compared to living systems, but they provide good control and allow detailed structural studies of membrane behaviour and interactions with relevant agents, such as proteins, peptides, and DNA [11].

Supported lipid bilayers (SLBs) are lipid bilayers formed on a solid substrate, most commonly silicon or quartz. Such supported bilayers provide a platform that is compatible with investigation using a range of interfacial science techniques including atomic force microscopy, attenuated total reflection infrared spectroscopy (ATR-IR), quartz crystal microbalance with dissipation (QCM-D) and neutron/X-ray reflectivity.

Several strategies for forming SLBs exist and have been thoroughly reviewed [12, 13, 14, 15]. The main approaches for SLB formation are the

Langmuir-Blodgett (LB) technique [16] and vesicle deposition [17]. Unlike the LB process, the formation of SLBs by vesicle deposition does not require specialist equipment, but vesicle and buffer conditions need to be optimised to achieve full coverage of the interface [18, 19]. Both techniques can form close-packed bilayers that are stable for many hours or days, allowing detailed measurements. The major disadvantage of SLBs is the proximity to the substrate: the lipid bilayers can experience strong interactions (e.g.van-der-Waals attraction) with the solid surface, restricting the natural bilayer fluctuations and influencing lipid phase behaviour and dynamics [20]. The lack of space between the bilayer and the substrate impedes the incorporation of membrane proteins. To circumvent this, tethered and floating bilayer approaches have been developed. Both of these approaches allow a fluid lipid bilayer layer to be formed that is not in direct physical contact with the underlying solid substrate. In the case of tethered bilayers, the tether still constrains the bilayer fluctuations. Floating supported lipid bilayers (FSBs) are typically formed by performing Langmuir-Blodgett (LB) deposition followed by Langmuir-Schaefer (LS) deposition onto a self-assembled monolayer (SAM)-functionalized solid substrate, although by using a charged SAM, they can also be formed by vesicle deposition [21]. Out-of-plane bilayer fluctuations provide an (entropic) steric repulsion which balances the van der Waals attraction between the bilayer and the substrate, resulting in a water layer between the SAM and bilayer of thickness that is typically in the range 30-50 Å [22]. The fluctuations mean that floating bilayers more closely resemble native biomembranes than supported bilayers [23]. Although recent work has demonstrated improvements in the stability of floating bilayers [21], the LB-LS process remains time and labour intensive and still has a relatively high failure rate.

Here, we describe the development of a *suspended bilayer* approach, which removes the presence of a solid substrate, and the concomitant constraint on membrane fluctuation, but retains the convenience of preparation by vesicle rupture [24]. In the suspended bilayer approach presented here, a cationic surfactant (DODAB) monolayer is spread at the air-water interface and vesicles comprising a mixture of zwitterionic (POPC) and anionic (POPG) lipids are osmotically ruptured beneath the monolayer to form planar bilayers. We use a 3:1 mixture of POPC:POPG in order to form a bilayer that has a comparable charge density to that of the inner membrane of Gram negative bacteria, using POPC rather than POPE to obtain a bilayer with an intrinsic curvature of zero [25, 26]. Separately, we found that we could perform

cell-free expression of the bacterial ion channel MscL into vesicles of this composition and the resulting proteoliposomes can be used to form similar suspended bilayers that incorporate the protein [27].

Vesicle adsorption is initiated from a buffer containing 150 mM NaCl. This concentration is sufficiently high to screen vesicle-vesicle repulsion during assembly at the interface, whilst being low enough to allow for small (100 nm diameter) unilamellar vesicles to remain suspended in solution. It is comparable to the concentrations (100 mM and 150 mM) used in other studies involving vesicle rupture [28, 29, 30].

Formation of a high coverage lipid bilayer is dependent on vesicle rupture. On solid substrates, vesicle rupture is driven by a balance between the vesicle-to-substrate adhesion energy, the bending energy of the lipid bilayer and an energy associated with the osmotic stress across the bilayer [31, 28, 32]. Each of these energies is impacted by lipid composition, vesicle diameter, ionic concentration, temperature, nature of the substrate and the specific adsorption of cations [33]. In the case of the suspended bilayer system presented here, the attractive interaction between the monolayer and the vesicle is likely driven by counterion release [34, 35].

We found the monolayer-vesicle attraction to be insufficient for complete rupture of the vesicles on adsorption at this interface and use changes in the salt concentration of the sub-phase buffer to osmotically rupture adsorbed vesicles. Exchanging the sub-phase such that the concentration of NaCl outside the adsorbed vesicles is higher than that inside the vesicles provides a driving force for vesicle rupture. As the vesicle bilayer is more permeable to water than to salt, the osmotic imbalance leads to an efflux of water from the vesicles. The accompanying decrease in vesicle volume results in a membrane tension causing deformation and vesicle fusion [36, 37, 38]. A second change in salt concentration, returning to a lower salt concentration, was required for vesicle rupture at the air-water interface. Reduction of the salt concentration decreased the distance between the larger fused vesicles (with larger contact area than the original vesicles) and the monolayer and increased the internal volume of the fused vesicles resulting in vesicle rupture to a planar bilayer.

The suspended bilayer model presented here is a membrane architecture which employs a surfactant monolayer at the air-water interface. The monolayer takes the role of the self-assembled monolayer in floating supported bilayers and contributes to the balance of forces that allows a lipid bilayer to be suspended underneath the monolayer.

2. Materials & methods

2.1. Materials

DODAB (Dimethyldioctadecylammonium bromide) was obtained from Sigma Aldrich; POPC (1-palmitoyl-2-oleoyl-sn-glycero-3-phosphocholine) and POPG (1-palmitoyl-2-oleoyl-sn-glycero-3-phospho-(1'-rac-glycerol) (sodium salt)) were obtained from Avanti Polar lipids as powders and used without further purification. Components for buffer solution and ethanol were purchased from Sigma Aldrich.

2.2. Methods

2.2.1. Vesicle preparation

3:1 POPC:POPG vesicles were prepared by dissolving a 3:1 mixture of POPC and POPG lipids in the minimum amount of chloroform, evaporating the chloroform under a steady stream of nitrogen and rehydrating the lipid film in HEPES buffer (20 mM HEPES, pH 7.4, 150 mM NaCl). To ensure unilamellar vesicles of diameter ∼100 nm, the lipid solution was then sonicated at room temperature for 30 minutes before being extruded through 100 nm filters using the Avanti mini-extruder, a minimum of 11 times, after which the vesicle solution became transparent and opalescent. At this stage the concentration of NaCl is 150 mM both inside and outside the vesicles.

2.2.2. Neutron Reflectivity (NR)

Neutron reflectivity measurements were carried out using the INTER reflectometer at the ISIS spallation source, Rutherford Appleton Laboratory (Oxfordshire, UK). A broad band neutron beam with wavelengths from 1.5 to 15 Å was used. The reflected intensity is measured as a function of the momentum transfer $Q_z = \frac{4\pi}{\lambda}\sin\theta$, where λ is wavelength and θ is the incident angle. The collimated neutron beam was reflected from the air-liquid interface at glancing angles of $\theta = 0.8$ and 2.3° in order to cover the desired Q range, from the total reflection edge to where the reflectivity falls to the background. The total illuminated area was 15 by 65 mm, allowing the reflectivity to be measured for $0.011 \leq Q_z \leq 0.29$ Å^{-1} at a resolution $\Delta Q_z/Q_z = 5\%$. All neutron reflectivity measurements were conducted at 21°C.

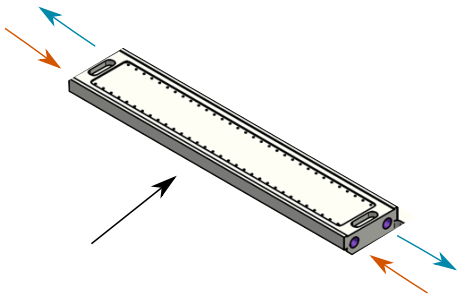

Figure 1: Drawing of the laminar flow trough design. Red arrows indicate the inlets through which liquids are pushed in and blue arrows indicate inlets through which liquid is pulled out through PTFE Omnifit tubing using a syringe pump in push-pull mode. Large black arrow indicates the direction of the laminar flow across the trough.

2.2.3. Trough Design

A specifically designed PTFE laminar flow trough, a drawing of which is shown in Figure 1, was used for the formation of the suspended bilayers. The trough has dimensions 24 mm by 160 mm and a depth of 0.5 mm. The volume of the trough is 10 mL, which includes the liquid contained in the meniscus. The Supplementary Information contains a technical drawing of the trough. The trough design has been subsequently modified to include a barrier to allow for monolayer compression and the capability for temperature control [39].

A syringe pump (World Precision Instrument, model SP210CZ) was used in push-pull mode to simultaneously inject liquid into an inlet channel (indicated by the red arrows in Figure 1) connected to the sub-phase by 32 $\times$ 2 mm diameter holes running along the length of one edge of the base of the trough, whilst withdrawing liquid through 32 $\times$ 2 mm diameter holes along the opposite edge of the base of the trough, connected to an outlet channel (indicated by blue arrows in Figure 1). At a flow rate of 2 mL min^{-1} the sub-phase can be exchanged without disturbing a surfactant monolayer adsorbed at the interface, as illustrated schematically in Figure 2.

2.2.4. Formation of Suspended Bilayers

The trough was cleaned with ethanol, Milli-Q water and finally with chloroform prior to the experiment. The trough was first filled with the

buffer (20 mM HEPES, 150 mM NaCl in D_2O at pD 7). A solution of 2 mg mL^{-1} DODAB in chloroform was spread on an aspirated buffer surface to a surface pressure of 27–28 mN m^{-1} measured using a Wilhelmy plate.

The sub-phase was exchanged by passing fresh D_2O buffer through the laminar trough, underneath the monolayer, to remove any surfactant that had entered the sub-phase during the spreading of the monolayer, before measuring the specular neutron reflectivity. To form the suspended bilayer, 20 mL of a 1 mg mL^{-1} vesicle solution was flowed through the trough, underneath the surfactant monolayer, at a flow rate of 2 mL min^{-1} using two coupled syringes in a syringe pump in push-pull mode. To allow for diffusion of vesicles across the stagnation layer beneath the monolayer, the vesicle solution was left for 2 hours (in the first bilayer formation protocol) and 1 hour (in the second bilayer formation protocol) after vesicle injection before flowing solutions of 300 and then 150 mM NaCl in 20 mM HEPES buffer in D_2O at pD 7 through the trough, to trigger rupture of vesicles by osmotic shock.

2.2.5. Neutron Reflectivity Data Analysis

The structure of the suspended bilayer was determined by finding the parameters that minimized the χ^2 calculated between the measured reflectivity and that calculated for a model, based on Figure 2. The minimum χ^2 was found using the differential evolution algorithm within the Rascal 2.0 MatLab package.[40] From the air-water interface into the sub-phase, the model (fit parameters given in parentheses) comprises: a single layer description of the DODAB monolayer (monolayer hydration, DODAB area per molecule, monolayer roughness); a water layer (water gap thickness); a four layer description of the lipid bilayer, comprising lipid head group/tail layers for symmetrical outer and inner leaflets. The details of the calculation of the layer thicknesses and scattering length densities are given in the Supplementary Information. The monolayer is close to being contrast-matched to air, making the fit insensitive to the structural details of this layer. The measured surface pressure of of 27–28 mN m^{-1} provides strong evidence for the presence of the monolayer, so we include it in the model, but with the APM of the DODAB molecules constrained to the range 65 to 95 $Å^2 molecule^{-1}$, as determined from the amount of DODAB spread in the monolayer. In the Supplementary Information (SI section V.A.) we show that the inclusion of this layer only affects the best fit value determined for the number of water molecules per lipid head.

To fit the data measured during the formation of the lipid bilayer shown

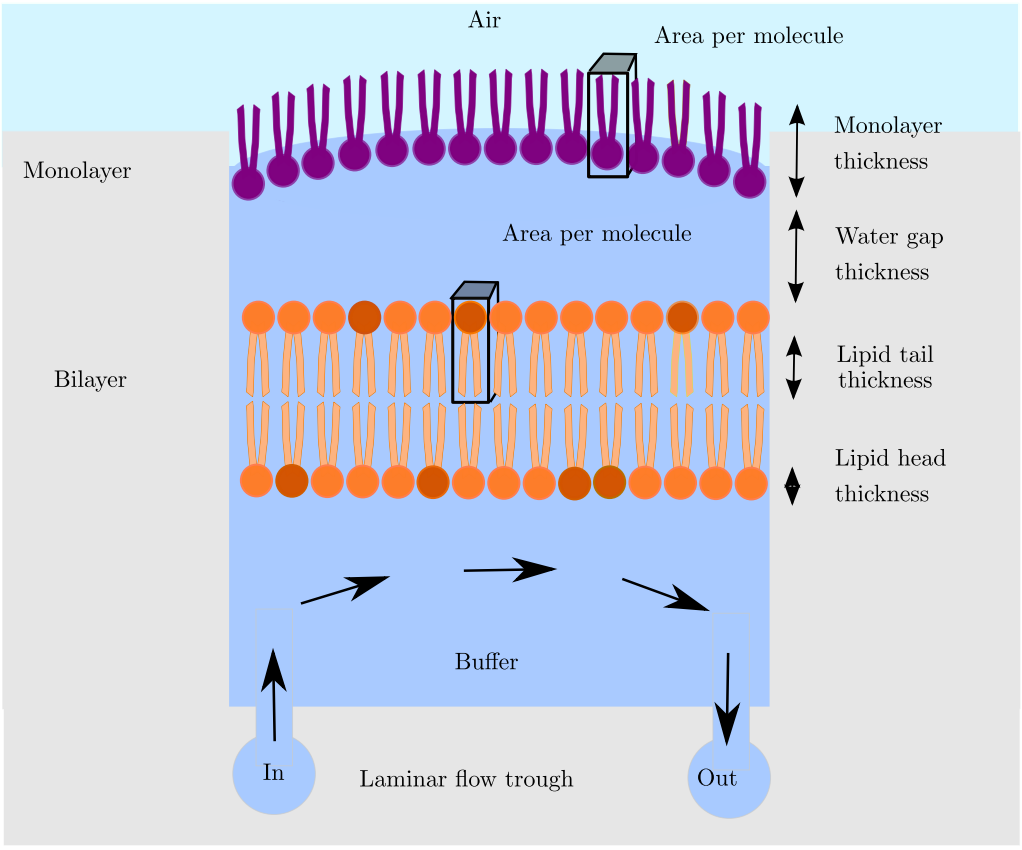

Figure 2: Schematic of the suspended lipid bilayer geometry illustrating key structural parameters used in the model to fit the measured neutron reflectivity and how the buffer sub-phase is exchanged by laminar flow. Note that bilayer and trough relative dimensions are not to scale.

in Figure 4, rather than allowing only the head-group layer to incorporate water (characterized as n_w water molecules per lipid head group), we allow for the whole bilayer to incorporate water (characterizing the hydration as a percentage of the volume of the bilayer occupied by water). As we demonstrate in the Supplementary Information (SI section V.B) it is necessary to include a second bilayer separated from that directly beneath the DODAB monolayer for the model to be able to describe the reflectivity measurements shown in the middle 3 panels of Figure 4, which were measured at intermediate stages of bilayer formation protocol 1. To describe the reflectivity measured in stage 4 of the formation process, this second bilayer is replaced

by a highly hydrated diffuse lipid layer.

3. Results & discussion

3.1. Results

Our aim was to form a phospholipid bilayer underneath a surfactant monolayer by exploiting the driving force for vesicle adsorption and rupture associated with counterion release arising from the difference in the sign of the charge associated with the positively charged DODAB molecules in the monolayer and the negatively charged (3:1 POPC:POPG) vesicles. The requirement for a difference in the sign of the charge between the monolayer and the vesicles was confirmed by the reflection-absorption infrared spectroscopy (RAIRS) measurements shown in the Supplementary Information. These measurements indicated that the adsorption of vesicles comprising only zwitterionic POPC was substantially less than for the 3:1 POPC:POPG vesicles that form the basis of our bacterial membrane mimetic.

The assembly of a vesicle layer and subsequent rearrangement into a bilayer structure underneath the surfactant monolayer was investigated with neutron reflectivity.

3.1.1. Structures determined during bilayer formation protocol 1

Neutron reflectivity was measured for $0.01 \leq Q \leq 0.11$ Å^{-1} for 45 minutes starting from the start of an injection of 20 mL of a 1 mg mL^{-1} dispersion of vesicles at a rate of 1 mL min^{-1}. This data was time-sliced into 3 minute segments as shown in Figure 3. Eighteen minutes after the start of the vesicle injection, the neutron reflectivity profile began to change drastically with the emergence of two clear minima at 0.023 and 0.055 Å^{-1}. After $\sim$ 36 minutes, the rate of change in the reflectivity profile decreases, corresponding to a decrease in the rate at which the interfacial structure is changing.

The material is not initially distributed as a single bilayer, and a highly hydrated double bilayer model provides the best fit to the measured reflectivity. This model is constructed from 9 layers arranged from the air-water interface into the sub-phase as: a DODAB layer, a water layer ($W1$); head group, tail and head group layers for the first bilayer ($B1$); a second water-rich layer ($W2$); and another sequence of head group, tail and head group layers forming a second bilayer layer ($B2$). The best fit area per molecule (APM) values from which the bilayer thicknesses (T_{B1} and T_{B2}) were calculated and the best fit water layer thicknesses (T_{W1} and T_{W2}) and hydration

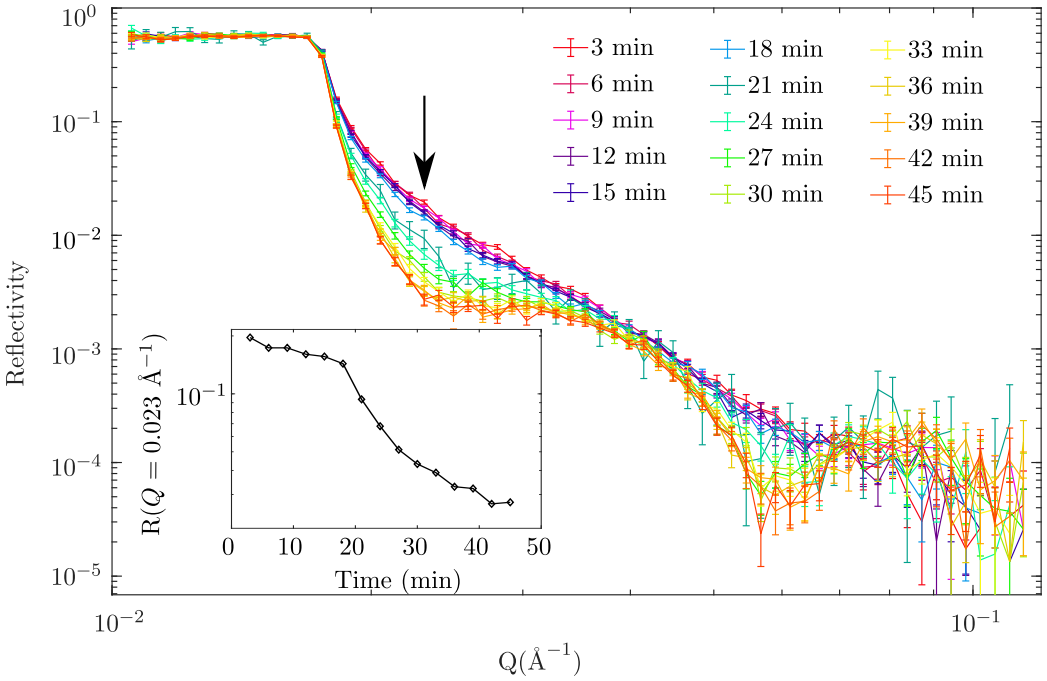

Figure 3: Neutron reflectivity measured during the assembly of 3:1 POPC:POPG vesicles underneath a DODAB surfactant monolayer. Injection of 20 mL of a dispersion of vesicles at a rate of 1 mL min^{-1} starts at 0 minutes and is sufficient to replace the sub-phase volume twice over. The inset plot shows the reflectivity measured at Q=0.023 Å^{-1} as a function of time; this value of Q is indicated on the main plot by the arrow.

of the bilayers (H_{B1} and H_{B2}) are summarised in Table 1. See the Supplementary Information for details on the calculation of layer thicknesses and scattering length densities from the model parameters. The best fits to the reflectivity profiles measured for the D_2O based buffer during the 4 stages of bilayer formation are shown as the left column in Figure 4, with the corresponding scattering length density (SLD) profiles shown in the middle column, and a schematic interpretation of the structure shown in the right column. The best fit model parameters for these fits are displayed in the Supplementary Information. In Figure 4 and Table 1, stages 1 and 2 correspond to 1 hour and 1.5 hours after the start of the vesicle injection respectively, stage 3 is after stepping the NaCl concentration up to 300 mM and stage 4 is after the NaCl concentration has been stepped back down to 150 mM. As we show in the Supplementary Information (SI section V.B.), to fit the reflectivity shown in the middle three rows of Figure 4 requires a double

Table 1: Summary of the key best fit parameters used to fit the neutron reflectometry profiles measured during different stages of the formation of a suspended lipid bilayer, with the upper and lower bounds of the 65% confidence interval given in square brackets. Stages 1 and 2 correspond to 1 hour and 1.5 hours after the start of the vesicle injection, respectively; stage 3 is after stepping the NaCl concentration up to 300 mM; stage 4 is after the NaCl concentration has been stepped back down to 150 mM. *Note that in stage 4, T_{B2} and H_{B2} denote the thickness and hydration of the diffuse layer depicted in Figure 4. A full listing of the best fit parameters, confidence intervals and the bounds used in the fitting procedure can be found in Tables S3 to S6 in the Supplementary Information.

Formation Stage	T_{W1} (Å)	T_{B1} (Å)	H_{B1} (%)	T_{W2} (Å)	T_{B2} (Å)	H_{B2} (%)
1	26[24 28]	17[15 23]	21[17 40]	66[65 70]	28[26 39]	30[24 39]
2	27[25 30]	31[28 45]	21[2 29]	45[42 54]	31[28 45]	23[1 30]
3	37[34 38]	19[18 20]	10[2 14]	30[26 36]	27[23 34]	47[39 49]
4	10[8 12]	44[42 46]	5[0 6]	52[31 64]	146[124 165]*	90[89 92]*

bilayer structure, which we attribute to vesicles flattened into pancake-like structures by strong adhesion. During these intermediate stages, the SLD profile in the $W2$ layer, between the bilayers, remains below the SLD of the sub-phase. This is likely due to the presence of some lipid from the rims of the pancake-like structures, adding a contribution to the bilayer roughnesses. The reflectivity in the bottom row of Figure 4, has been fit to a single well-defined bilayer, plus a thicker, highly hydrated diffuse lipid layer. In the Discussion (section 3.2.2) we discuss a possible mechanism for the development of the structures depicted schematically in Figure 4.

3.1.2. Structure of final suspended bilayer formed by protocol 2

In a second bilayer formation protocol, we reduced the time between starting vesicle injection (stage 1) and the step up in NaCl concentration to 300 mM (stage 3) from 2 hours to 1 hour. The reflectivity profiles measured in both D_2O and a 35% D_2O/65% H_2O mixture buffer (SLD = 2.8×10^{-6} Å^{-2}) at the end of stage 4 of this modified procedure is shown in Figure 5. The best fit to the reflectivity is provided by a single high coverage bilayer beneath the DODAB monolayer. This means that initiating the final rupture of the vesicles earlier than in protocol 1 had the desired effect of allowing a complete bilayer to form, without the excess unruptured vesicles. Table 2 gives the best fit parameters determined by co-refining the two profiles to the single bilayer model, which was constrained according to the parameter

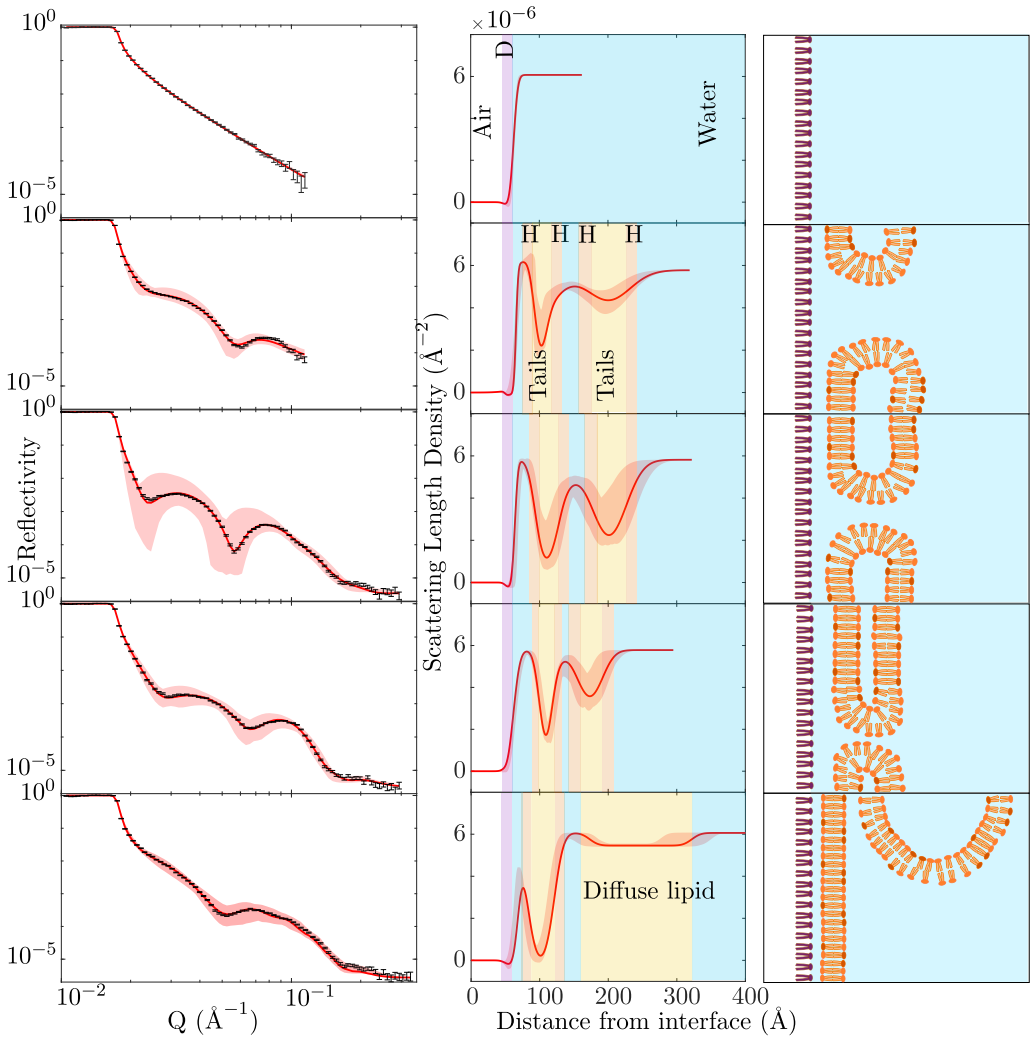

Figure 4: Fitted neutron reflectivity profiles, corresponding SLD profiles and schematic representations of the interfacial structures for: a DODAB monolayer (top); stages of vesicle adsorption and deformation (middle three panels); and vesicle rupture after stepping the NaCl concentration back down to 150 mM (bottom). The reflectivity data points are depicted by the error bars (black) denoting the measurement uncertainty. The χ^2 best fits are shown as red lines with red shading, denoting 65% confidence interval bands calculated from Bayesian analysis. H = head group layers of the lipid bilayers. D= DODAB monolayer. We emphasize that the cartoon representations shown in the right panel, do not attempt to accurately depict the in-plane extent of the pancake-like structures in the middle 3 rows or the the coverage of the intact vesicles that we suggest are responsible for the diffuse layer.

bounds also given in Table 2 . An MCMC analysis was applied to determine the 65% confidence intervals for the parameters of the model, which are shown in Table 2 . The fit to the data and corresponding scattering length density profiles are shown in Figure 5.

Table 2: Best fit model parameters used to fit neutron reflectivity profiles measured from a 3:1 POPC:POPG lipid bilayer suspended underneath a surfactant monolayer, with the lower and upper bounds on the 65% confidence intervals calculated from Bayesian analysis shown in square brackets.

Parameter	Parameter Bounds	Fitted Value	65% Confidence Interval
Bilayer roughness(Å)	[2 10]	9	[8.4 9.7]
APM of bilayer(Å^2 molecule^{-1})	[50 120]	58	[56.0 59.5]
Water Gap (Å)	[0 40]	11	[9.3 14.7]
Water per lipid head	[0 18]	8	[0 10]
Surface roughness(Å)	[2 7]	5	[4.3 6.6]
APM of monolayer(Å^2 molecule^{-1})	[65 95]	83	[65.4 88.6]
Monolayer hydration (%)	[0 15]	7	[0.0 8.9]

The best-fit bilayer structure has a roughness of 9 Å, which is larger than is typically observed for solid-supported bilayers [41]. This is consistent with the suspended bilayers exhibiting larger amplitude out-of-plane fluctuations than solid-supported bilayers. The separation between the monolayer and the bilayer is determined by the balance between the attractive interaction, associated with counterion release, and steric repulsions associated with the out-of-plane fluctuations [42], and hydration repulsion [43]. We note that in the analysis of the grazing incidence X-ray scattering from a DMPC-DMPG bilayer adsorbed beneath a Langmuir monolayer at the air-water interface, Pusterla *et al.* convolute the electron density profile with a Gaussian of width 10 Å, to account for the roughness of the bilayer associated with such out-of-plane fluctuations [44]. The 10 Å thickness for the water layer between the bilayer and the monolayer at the air-water interface they observe is also very similar to the 11 Å gap we observe, although their measurements are from a bilayer with a coverage of 50%.

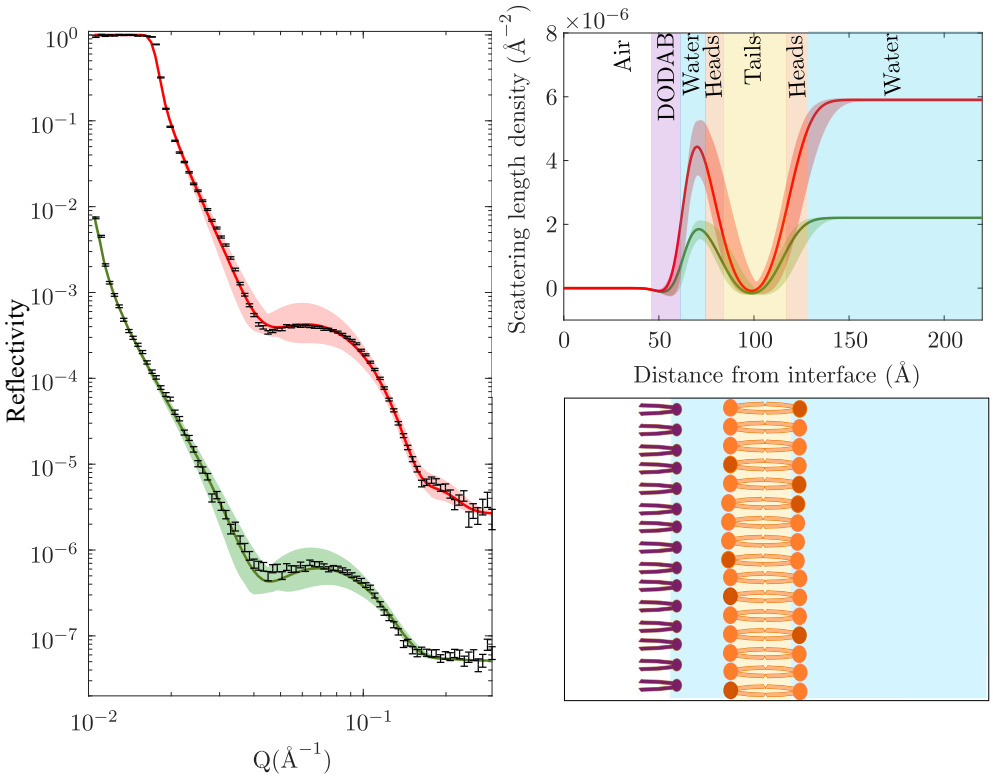

Figure 5: Left panel: Neutron reflectivity profiles measured (data points shown as black error bars) from the final suspended lipid bilayer resulting from formation protocol 2 in D_2O buffer shown in red and 35% D_2O buffer shown in green (offset on vertical axis for clarity); the best fits to the data are shown as solid lines and the shaded band gives the 65% confidence interval. Top right: scattering length density profiles corresponding to the fits in left panel. Bottom right: schematic representation of the structure corresponding to the scattering length density profile of the suspended bilayer.

3.2. Discussion

3.2.1. Characterisation of the final suspended bilayer

The model we use to fit the reflectivity profiles measured in two contrasts from the final bilayer structure formed by protocol 2 contains the seven parameters listed in Table 2. The posterior probability distributions given in Figure S4 of the Supplementary Information, show that the fit is most sensitive to the area per lipid molecule (APM) in the bilayer and the thickness of the water layer between the monolayer and the bilayer, whereas it is less sensitive to the hydration and hence thickness of the bilayer head group layer. These relative parameter sensitivities, suggest that the suspended bilayer approach should be well-suited to investigating either changes in lipid packing density or the insertion of membrane-spanning proteins, such as ion channels. Conversely, it might be less well-suited to investigating insertion of molecules into the lipid head group region.

Experimentally determined values for the APM of POPC in bilayers range from 62.7± 1.3 Å^2, determined using small-angle scattering from $\sim$ 600 Å diameter unilamellar vesicles [45], to 85 ± 23 Å^2, determined using neutron reflectivity from floating bilayers [46]. For POPG, an APM of 64.4 ± 0.2 Å^2 has been determined using small-angle scattering [47]. Molecular dynamics simulations, suggest that at 150 mM NaCl the APM for a POPG bilayer is 54.8±0.4 Å whilst a POPC bilayer would have an APM of 64.1± 0.6 Å^2 [48]. Using these values, and assuming ideal mixing of POPC and POPG in the 3:1 ratio we use to form the suspended bilayers, one might predict an average APM for a 3:1 POPC/POPG bilayer of 62 Å^2, which is close to the best fit value we determine of 58 ± 2 Å^2. As the bilayer is unconstrained by any interaction with a solid substrate, the suspended bilayer system provides an ideal experimental system with which to compare the results from molecular dynamics simulations.

We emphasize that the model that provides the best fit to the reflectivity profiles shown in Figure 5 corresponds to a 100% coverage bilayer, with no water incorporated into the tail region, and that this high coverage bilayer covers the large area beneath the air-water interface of the trough.

3.2.2. Vesicle adhesion and rupture

The data we measured during formation protocol 1 (Figure 4) shows sufficiently well-defined changes in the reflectivity for us to be able to discuss a possible mechanism of bilayer formation. As is depicted schematically in Figure 6, adsorption of vesicles is driven by the attractive counterion

release interaction between the vesicles and the surfactant monolayer. The sequence of neutron reflectivity profiles shown in Figure 4 is consistent with a combination of the deformation and fusion mechanism described by Revikane & Brisson [49], which follows the physics described by Seifert [50], and the role for osmotic pressure described by Jackman *et al.* [28].

We suggest that the strong adhesion energy between the DODAB monolayer and the POPC:POPG vesicles, mediated by counterion release, is sufficient to flatten the adsorbed vesicles into the pancake-like structures predicted theoretically by Lipowsky & Seifert [51, 52] and by coarse-grained models [53]. In stage 1, the height of such a flattened vesicle would be $T_{B1} + T_{W2} + T_{B2} = 113$ Å. Using our estimate for the adhesion energy of $W_{ad} = 2.8$ mJ m^{-2} and a value for the bending rigidity $\kappa_b = 25\ k_BT$, we can use the expression derived by Seifert & Lipowsky [50] to predict the height of flattened POPC:POPG vesicles in 150 mM NaCl adsorbed underneath a DODAB covered air-water interface to be ~ 100 Å (see Supplementary Information for justification). This contrasts with the conclusion reached by Koutsiobas *et al.* that the interaction of headgroups of POPC vesicles with a silica surface (which will likely be weaker than in our system due to an absence of counterion-release) is insufficient to deform the vesicles enough for the double bilayer structure they infer from their reflectivity profiles to be be associated with opposing flattened faces of the same vesicle [54]. Instead they describe an interface that is decorated by patches of bilayer from ruptured vesicles, with intact vesicles adsorbing at the edges of these patches, resulting in a sigmoidal bilayer that conforms over the patch, like a rug covering a step (see Figure 10 of [54]).

The APM we determine for the first bilayer in stages 1-3, suggest that vesicle adhesion is accompanied by a lateral expansion (areal strain), visible as a thinning of the bilayer, which will promote fusion of the adsorbed vesicles. The decrease in the second water layer thickness from 45 Å to 30 Å on stepping up the salt concentration from 150 to 300 mM NaCl (stage 2→3) is consistent with the decrease in internal volume of the vesicles expected to accompany the efflux of water from the vesicles in response to the osmotic upshock. As the vesicles continue to flatten and spread laterally, further fusion of interacting vesicles will be promoted [49, 28]. The low thickness of the first bilayer (T_{B1}=19 Å) suggests that the bilayer is under a tension, which is relieved by osmotic rupture of any remaining curved interfaces at the perimeters of the pancake-like structures following the influx of water on stepping the salt concentration back down to 150 mM (stage 4). This results

in a well-defined bilayer separated from the monolayer by a 11 Å water layer. The structural signature of the formation of a complete suspended bilayer in the first bilayer formation protocol is the increase in the bilayer thickness from 19 to 44 Å which indicates a release of areal strain. The accompanying decrease in the thickness of the water layer between the surfactant monolayer and the first bilayer (T_{W1}) that occurs between stages 3 and 4 in Table 1 is consistent with an increase in the strength of the attractive interaction caused by a decrease in the electrostatic screening when the salt concentration is stepped down. This effect has been observed in other bilayer systems [21, 55] and, following the work of Jackman *et al.* [28], the increase in interaction strength would also be expected to contribute to the final rupturing any remaining curved interfaces at the perimeters of the pancake-like structures adsorbed beneath the monolayer.

A second lipid layer remained at this stage, but instead of a well-defined second bilayer it was necessary to include a diffuse lipid layer of thickness 146 Å, which we speculate can be ascribed to a low coverage of intact vesicles. We note that a scenario for stage 4 in which a single suspended bilayer covering most of the sub-phase face of the DODAB monolayer coexists with unruptured vesicles adsorbed directly beneath a small fraction of the DODAB monolayer, cannot be ruled out on the basis of fits to the specular reflectivity. The insensitivity of specular reflectivity to lateral structure and the fact that adhesion promotes fusion of the adsorbed vesicles [49, 28], also means that we are not able to determine the lateral size of the flattened vesicles at the various stages (1-3) of the formation protocol 1.

3.2.3. Comparing suspended bilayers to nanodisc assembly at the air-water interface

Previously Wadsäter *et al.* observed the formation of DMPC:DMPG SMALP nanodiscs underneath a DODAB monolayer at the air-water interface, also observing that a difference in charge is needed between the nanodisc lipids and the monolayer [56]. Our continuous suspended bilayer has the advantage of removing the need for any polymer in the bilayer region and still holds the potential of protein-incorporation into the lipid bilayer through proteoliposome rupture.

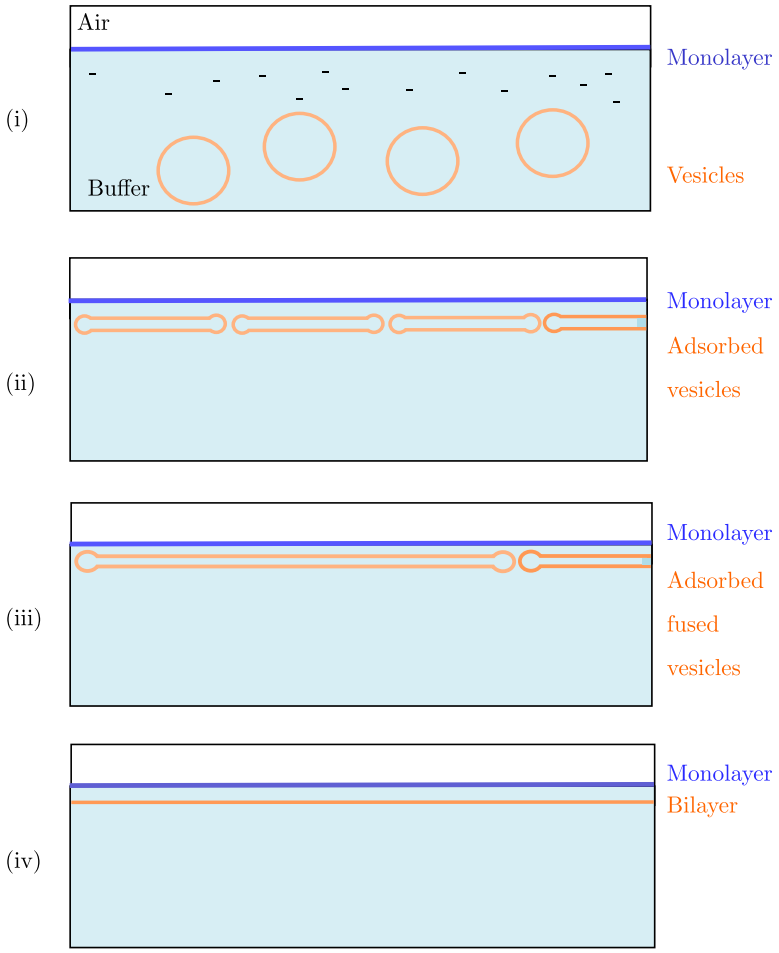

Figure 6: Proposed mechanism of vesicle rupture in the formation of a suspended lipid bilayer. i) Prior to the adsorption of vesicles under the monolayer, a charge gradient exists underneath the cationic surfactant monolayer with a higher concentration of anions associated at the air-water interface. ii) Vesicles adsorb underneath the monolayer and flatten to maximize the adhesive contribution to the free energy arising from counterion release. iii) After adding 300 mM NaCl buffer the decrease in internal volume that accompanies efflux of water promotes further flattening and fusion resulting in a decrease in the height of the pancake-like structure. iv) After returning to 150 mM NaCl buffer a single lipid bilayer suspended underneath the monolayer remains.

3.2.4. Suitability of suspended bilayer system to study inserted membrane proteins

We have found that the relatively unconstrained nature of the suspended bilayer and the presence of a water layer between the surfactant monolayer and the bilayer makes this a suitable platform with which to investigate bilayers incorporating membrane proteins [27]. The water layer provides the space to accommodate domains that protrude out from the membrane. In this context, we speculate that it should be possible to control the thickness of the water layer, by controlling the salt concentration, as has been found using floating bilayers [21, 55], enabling inclusion of proteins with large transmembrane domains.

3.3. Conclusions

Neutron reflectivity measurements have been used to show that vesicles comprising a 3:1 mixture of POPC:POPG adsorb beneath a DODAB monolayer spread at the air-water interface of a laminar flow trough. The attractive interaction, which is likely driven by counterion release, results in a flattening of the vesicles. The purpose-built laminar flow trough allows for a sequence of changes in the salt concentration of the buffer, which drive the complete rupture of the flattened vesicles resulting in the formation of a continuous bilayer suspended beneath the monolayer at 100% coverage.

The requirement for a difference in the sign of the charge associated with the monolayer and the lipid bilayer, that we confirmed by RAIRS, has also been noted by Wadsäter *et al.* in their study of DMPC:DMPG SMALP nanodiscs beneath a DODAB monolayer [56]. Pusterla *et al.* also make use of the attractive interaction between a monolayer containing cationic lipids and vesicles containing anionic lipids in forming bilayers adsorbed at functionalized air-water interfaces [44].

The measured neutron reflectivity profiles are easy to interpret, as the interfacial region does not feature any of the superfluous layers such as silicon, silicon dioxide or gold that are typically present for floating bilayers formed on solid substrates. The profiles are particularly sensitive to the thickness of the water layer between the monolayer and the bilayer and the APM of the lipids in the bilayer.

The location of the bilayer, 11 Å beneath the surfactant monolayer at the air-water interface, means that it can be conveniently be probed by a variety of surface science techniques, such as X-ray reflectivity, Brewster angle

microscopy, ellipsometry and RAIRS, in addition to neutron reflectivity, as well as providing the space to incorporate transmembrane proteins.

As the bilayer is not constrained by a solid substrate it is able to fluctuate more freely than solid-supported bilayers, resulting in a broader bilayer SLD profile than is typically determined for such supported bilayers. The absence of of a solid substrate and the relative ease of preparation makes the suspended bilayer an exciting new membrane mimetic, which is well-suited to investigating systems that incorporate transmembrane proteins.

Electronic Supplementary information

Electronic supplementary information (ESI), with reduced data sets, Rascal Matlab analysis files and model scripts, available at https://github.com/SAyscough/SuspendedLipidBilayer.

CRediT authorship contribution statement

Sophie E. Ayscough: Methodology; Investigation; Formal analysis; Writing – Original draft. **Maximilian W. A. Skoda:** Methodology; Investigation; Formal analysis; Writing – review & editing; Supervision; Funding acquisition. **Luke A. Clifton:** Resources; Investigation. **Simon Titmuss:** Conceptualization; Methodology; Investigation; Writing – review & editing; Supervision; Funding acquisition.

3.4. Acknowledgments

We thank ISIS for use of the INTER reflectometer (DOI: 10.5286/ISIS.E.RB1910569) and user labs including the ISIS Biolabs and for use of the iS50 Thermo-Nicolet Fourier Transform Infrared Spectrometer (FT-IR). We also thank Diamond Light Source for beamtime on IO7 (SI22995-1) that allowed for further testing of trough design and bilayer assembly (data not shown in this paper), with special thanks to Jonathan Rawle Instrument Scientist and Andrew McCluskey for data fitting discussions. We would also like to thank Jacob Simms, senior mechanical support technician at ISIS for aiding in the design and fabrication of our final reflectometry trough design, in particular for the technical drawings. We thank the mechanical workshop in the School of Physics & Astronomy, at the University of Edinburgh for fabrication of initial reflectometry trough prototypes. SA was supported by the EPSRC CDT on "Soft and Functional Interfaces" (EP/L015536/1) and an ISIS Facility Development Studentship. For the purpose of open access, the author has applied a Creative Commons Attribution

References

[1] D. Meleleo, Study of resveratrol's interaction with planar lipid models: Insights into its location in lipid bilayers, Membranes 11 (2021) 132.

[2] C. Peetla, R. Bhave, S. Vijayaraghavalu, A. Stine, E. Kooijman, V. Labhasetwar, Drug resistance in breast cancer cells: biophysical characterization of and doxorubicin interactions with membrane lipids, Molecular Pharmaceutics 7 (2010) 2334–2348.

[3] B. L. Kagan, M. E. Selsted, T. Ganz, R. I. Lehrer, Antimicrobial defensin peptides form voltage-dependent ion-permeable channels in planar lipid bilayer membranes, Proceedings of the National Academy of Sciences 87 (1990) 210–214.

[4] G. C. Troiano, L. Tung, V. Sharma, K. J. Stebe, The reduction in electroporation voltages by the addition of a surfactant to planar lipid bilayers, Biophysical Journal 75 (1998) 880–888.

[5] A. Maček Lebar, D. Miklavčič, M. Kotulska, P. Kramar, Water pores in planar lipid bilayers at fast and slow rise of transmembrane voltage, Membranes 11 (2021) 263.

[6] L. A. Clifton, M. W. Skoda, E. L. Daulton, A. V. Hughes, A. P. Le Brun, J. H. Lakey, S. A. Holt, Asymmetric phospholipid: lipopolysaccharide bilayers; a gram-negative bacterial outer membrane mimic, Journal of The Royal Society Interface 10 (2013) 20130810.

[7] C. Merz, W. Knoll, M. Textor, E. Reimhult, Formation of supported bacterial lipid membrane mimics, Biointerphases 3 (2008) FA41–FA50.

[8] N. P. Chongsiriwatana, A. E. Barron, Comparing bacterial membrane interactions of antimicrobial peptides and their mimics, in: Antimicrobial Peptides, Springer, 2010, pp. 171–182.

[9] G. Fragneto, Neutrons and model membranes, The European Physical Journal Special Topics 213 (2012) 327–342.

[10] J. Sarkis, V. Vié, Biomimetic models to investigate membrane biophysics affecting lipid–protein interaction, Frontiers in bioengineering and biotechnology 8 (2020) 270.

[11] L. E. McKinley, R. D. Barker, S. Titmuss, Neutron reflectivity as a tool for physics-based studies of model bacterial membranes, in: Advances in Experimental Medicine and Biology, volume 915, 2016, pp. 261–282.

[12] E. Sackmann, Supported membranes: scientific and practical applications, Science 271 (1996) 43–48.

[13] C. Steinem, A. Janshoff, W.-P. Ulrich, M. Sieber, H.-J. Galla, Impedance analysis of supported lipid bilayer membranes: a scrutiny of different preparation techniques, Biochimica et Biophysica Acta (BBA)-Biomembranes 1279 (1996) 169–180.

[14] G. Puu, I. Gustafson, Planar lipid bilayers on solid supports from liposomes–factors of importance for kinetics and stability, Biochimica et Biophysica Acta (BBA)-Biomembranes 1327 (1997) 149–161.

[15] E. T. Castellana, P. S. Cremer, Solid supported lipid bilayers: From biophysical studies to sensor design, Surface Science Reports 61 (2006) 429–444.

[16] A. Ulman, An Introduction to Ultrathin Organic Films: From Langmuir–Blodgett to Self–Assembly, Academic press, 2013.

[17] T. M. Bayerl, M. Bloom, Physical properties of single phospholipid bilayers adsorbed to micro glass beads. a new vesicular model system studied by 2H-nuclear magnetic resonance, Biophysical Journal 58 (1990) 357–362.

[18] T. K. Lind, M. W. Skoda, M. Cardenas, Formation and characterization of supported lipid bilayers composed of phosphatidylethanolamine and phosphatidylglycerol by vesicle fusion, a simple but relevant model for bacterial membranes, ACS Omega 4 (2019) 10687–10694.

[19] R. Richter, A. Mukhopadhyay, A. Brisson, Pathways of lipid vesicle deposition on solid surfaces: a combined $\mathrm{QCM}-\mathrm{D}$ and AFM study, Biophysical Journal 85 (2003) 3035–3047.

[20] Y. Gerelli, Phase transitions in a single supported phospholipid bilayer: Real-time determination by neutron reflectometry, Physical Review Letters 122 (2019) 248101.

[21] L. A. Clifton, N. Paracini, A. V. Hughes, J. H. Lakey, N.-J. Steinke, J. F. Cooper, M. Gavutis, M. W. Skoda, Self-assembled fluid phase floating membranes with tunable water interlayers, Langmuir 35 (2019) 13735–13744.

[22] A. V. Hughes, J. R. Howse, A. Dabkowska, R. A. Jones, M. J. Lawrence, S. J. Roser, Floating lipid bilayers deposited on chemically grafted phosphatidylcholine surfaces, Langmuir 24 (2008) 1989–1999.

[23] T. Charitat, E. Bellet-Amalric, G. Fragneto, F. Graner, Adsorbed and free lipid bilayers at the solid-liquid interface, The European Physical Journal B-Condensed Matter and Complex Systems 8 (1999) 583–593.

[24] M. Eeman, M. Deleu, From biological membranes to biomimetic model membranes, Biotechnologie, Agronomie, Société et Environnement 14 (2010) 719–736.

[25] S. G. Wilkinson, Bacterial lipopolysaccharides—themes and variations, Progress in Lipid Research 35 (1996) 283–343.

[26] R. Leber, M. Pachler, I. Kabelka, I. Svoboda, D. Enkoller, R. Vácha, K. Lohner, G. Pabst, Synergism of antimicrobial frog peptides couples to membrane intrinsic curvature strain, Biophysical Journal 114 (2018) 1945–1954.

[27] S. Ayscough, Investigation of the bacterial mechanosensitive ion channel of large conductance within bacterial membrane mimetics in response to simple antimicrobial molecules, Ph.D. thesis, University of Edinburgh, 2021.

[28] J. A. Jackman, J.-H. Choi, V. P. Zhdanov, N.-J. Cho, Influence of osmotic pressure on adhesion of lipid vesicles to solid supports, Langmuir 29 (2013) 11375–11384.

[29] H. P. Wacklin, Composition and asymmetry in supported membranes formed by vesicle fusion, Langmuir 27 (2011) 7698–7707.

[30] B. Seantier, B. Kasemo, Influence of mono-and divalent ions on the formation of supported phospholipid bilayers via vesicle adsorption, Langmuir 25 (2009) 5767–5772.

[31] T. K. Lind, M. Cárdenas, Understanding the formation of supported lipid bilayers via vesicle fusion—a case that exemplifies the need for the complementary method approach, Biointerphases 11 (2016) 020801.

[32] T. Zhu, Z. Jiang, E. M. R. Nurlybaeva, J. Sheng, Y. Ma, Effect of osmotic stress on membrane fusion on solid substrate, Langmuir 29 (2013) 6377–6385.

[33] E. Reimhult, F. Höök, B. Kasemo, Vesicle adsorption on SiO_2 and TiO_2: dependence on vesicle size, The Journal of Chemical Physics 117 (2002) 7401–7404.

[34] K. Wagner, D. Harries, S. May, V. Kahl, J. Rädler, A. Ben-Shaul, Direct evidence for counterion release upon cationic lipid- dna condensation, Langmuir 16 (2000) 303–306.

[35] M. T. Record, C. F. Anderson, T. M. Lohman, Thermodynamic analysis of ion effects on the binding and conformational equilibria of proteins and nucleic acids: the roles of ion association or release, screening, and ion effects on water activity, Quarterly Reviews of Biophysics 11 (1978) 103–178.

[36] M. Koslov, V. Markin, A theory of osmotic lysis of lipid vesicles, Journal of Theoretical Biology 109 (1984) 17–39.

[37] C. Vanhille-Campos, A. Šarić, Modelling the dynamics of vesicle reshaping and scission under osmotic shocks, Soft Matter 17 (2021) 3798–3806.

[38] G. J. Hardy, R. Nayak, S. Zauscher, Model cell membranes: Techniques to form complex biomimetic supported lipid bilayers via vesicle fusion, Current Opinion in Colloid & Interface Science 18 (2013) 448–458.

[39] B. Woden, M. W. Skoda, A. Milsom, C. Gubb, A. Maestro, J. Tellam, C. Pfrang, Ozonolysis of fatty acid monolayers at the air–water interface: organic films may persist at the surface of atmospheric aerosols, Atmospheric Chemistry and Physics 21 (2021) 1325–1340.

[40] A. Hughes, Rascal matlab application for analysis of neutron and x-ray reflectivity., 2020. https://sourceforge.net/projects/rscl/.

[41] H. P. Vacklin, F. Tiberg, G. Fragneto, R. K. Thomas, Composition of supported model membranes determined by neutron reflection, Langmuir 21 (2005) 2827–2837.

[42] W. Helfrich, Steric interaction of fluid membranes in multilayer systems, Zeitschrift für Naturforschung A 33 (1978) 305–315.

[43] J. N. Israelachvili, Intermolecular & Surface Forces, Academic Press, 2011.

[44] J. Pusterla, E. Scoppola, C. Appel, T. Mukhina, C. Shen, G. Brezesinski, E. Schneck, Characterization of lipid bilayers adsorbed to functionalized air/water interfaces, Nanoscale 14 (2022) 15048. URL: http://dx.doi.org/10.1039/D2NR03334H. doi:10.1039/D2NR03334H.

[45] N. Kučerka, M.-P. Nieh, J. Katsaras, Fluid phase lipid areas and bilayer thicknesses of commonly used phosphatidylcholines as a function of temperature, Biochimica et Biophysica Acta (BBA)-Biomembranes 1808 (2011) 2761–2771.

[46] A. V. Hughes, S. A. Holt, E. Daulton, A. Soliakov, T. R. Charlton, S. J. Roser, J. H. Lakey, High coverage fluid-phase floating lipid bilayers supported by ω-thiolipid self-assembled monolayers, Journal of The Royal Society Interface 11 (2014) 20140447.

[47] J. Pan, F. A. Heberle, S. Tristram-Nagle, M. Szymanski, M. Koepfinger, J. Katsaras, N. Kučerka, Molecular structures of fluid phase phosphatidylglycerol bilayers as determined by small angle neutron and x-ray scattering, Biochimica et Biophysica Acta (BBA)-Biomembranes 1818 (2012) 2135–2148.

[48] A. Dickey, R. Faller, Examining the contributions of lipid shape and headgroup charge on bilayer behavior, Biophysical Journal 95 (2008) 2636–2646.

[49] I. Reviakine, A. Brisson, Formation of supported phospholipid bilayers from unilamellar vesicles investigated by atomic force microscopy, Langmuir 16 (2000) 1806–1815.

[50] U. Seifert, R. Lipowsky, Adhesion of vesicles, Physical Review A 42 (1990) 4768.

[51] R. Lipowsky, U. Seifert, Adhesion of vesicles and membranes, Molecular Crystals and Liquid Crystals 202 (1991) 17–25.

[52] U. Seifert, Configurations of fluid membranes and vesicles, Advances in Physics 46 (1997) 13–137.

[53] K. Dimitrievski, Deformation of adsorbed lipid vesicles as a function of vesicle size, Langmuir 26 (2010) 3008–3011.

[54] A. Koutsioubas, M.-S. Appavou, D. Lairez, Time-resolved neutron reflectivity during supported membrane formation by vesicle fusion, Langmuir 33 (2017) 10598–10605.

[55] L. H. John, G. M. Preston, M. S. Sansom, L. A. Clifton, Large scale model lipid membrane movement induced by a cation switch, Journal of Colloid and Interface Science 596 (2021) 297–311.

[56] M. Wädsater, J. B. Simonsen, T. Lauridsen, E. G. Tveten, P. Naur, T. Bjornholm, H. Wacklin, K. Mortensen, L. Arleth, R. Feidenhans, et al., Aligning nanodiscs at the air–water interface, a neutron reflectivity study, Langmuir 27 (2011) 15065–15073.